



EUROPEAN COMMISSION
5th EURATOM FRAMEWORK PROGRAMME 1998-2002
KEY ACTION : NUCLEAR FISSION

HTR-E

High-Temperature Reactor Components and Systems

CONTRACT N°
FIKI-CT-2001-00177

Work Package 1
Hot gas duct configuration trade-off

MAB,ABP

Empresarios Agrupados

Spain

Contributors :
L. Briottet (CEA)

Dissemination level : RE
Document N° : HTR-E-03/11D-1-1-5-2
Status : Final

Empresarios Agrupados identification N° : 092-110-E-M-00002 issue 0



EUROPEAN COMMISSION

Project:

**HIGH TEMPERATURE REACTOR
COMPONENTS AND SYSTEMS (HTR-E)**

Title:

HTR Hot Gas Duct Configuration Trade-off

Document No: 092-110-E-M-00002	Issue: 0
Purpose of issue: Information and Comments	Date: 22/09/03

Prepared: MAB, ABP

Reviewed: AOM

Approved: MDB

This document contains proprietary information of Empresarios Agrupados Internacional, S.A. and is to be used solely for the Project and the purpose for which it is furnished. It may not be disclosed to others for a different use without the written permission of Empresarios Agrupados Internacional, S.A.



EMPRESARIOS AGRUPADOS

EMPRESARIOS AGRUPADOS INTERNACIONAL, S.A.

Magallanes, 3 28015 Madrid - España

CLASSIFICATION

Contains information for the design of structures, systems or components: Yes No

Design verification : Not applicable Head of OU/Supervisor Verifier Level 1 Level 2

CONTROL OF MODIFICATIONS

Issue	Modifications
0	Preliminary issue

PRELIMINARY OR PENDING INFORMATION

Issue	Paragraphs	Subject	Status

DISTRIBUTION

External	Internal	No. copies/Format
	MDB, AOM, ABP, MAB, AGD	1/ Hardcopy

CONTENTS

	Page No.
1. PURPOSE.....	1-1
2. INTRODUCTION.....	2-1
3. CALCULATION HYPOTHESES.....	3-1
3.1 REFERENCE HOT GAS DUCT	3-1
3.2 MATERIAL PROPERTIES.....	3-1
3.3 LOAD CASES CONSIDERED.....	3-2
3.4 PRESSURE DROP IN THERMAL INSULATION	3-3
3.5 He VELOCITY DURING PRESSURE DROP	3-4
4. CONNECTING SPACERS BETWEEN SUPPORT TUBE AND LINER	4-1
4.1 GEOMETRICAL CONFIGURATIONS STUDIED	4-1
4.2 THERMAL STRESSES ON THE SPACERS.....	4-2
4.3 STRUCTURAL STIFFNESS OF THE SPACERS.....	4-5
4.4 HEAT TRANSFERRED THROUGH THE INSULATION.....	4-6
4.5 CONCLUSIONS FOR THE DESIGN OF THE SPACERS.....	4-7
5. FIBRE FILTERING DURING PRESSURE DROP	5-1
5.1 GEOMETRICAL CONFIGURATIONS OF FILTERS STUDIED.....	5-1
5.2 PRESSURE DROP IN THE INSULATING CHAMBER.....	5-2
5.3 STRESSES ON THE FILTER STRUCTURE.....	5-4
6. CONCLUSIONS.....	6-1
7. REFERENCES.....	7-1
APPENDIX A FIGURES	7-1
APPENDIX B F.E.M FIGURES	

LIST OF ABBREVIATIONS

GT-MHR	Gas Turbine – Modular Helium Reactor
He	Helium
HP	High Pressure
HTR	High Temperature Reactor
LP	Low Pressure
PBMR	Pebble Bed Modular Reactor
PCU	Power Conversion Unit

1. PURPOSE

The purpose of this document is to present the trade off of the HTR hot gas duct.

The studies performed cover the different configurations for spacers between the support tube and the liner. In these studies, some alternatives for the components that serve as a filter during He pressure drop have been considered.

This report is Empresarios Agrupados' contribution to Deliverable 7b, "Thermal insulation of the turbine inlet" of HTR-E, WP1, "Turbine".

2. INTRODUCTION

The hot gas duct is part of the reactor Power Conversion Unit (PCU). It is the component that connects the HTR Module Reactor and the helium turbine.

The purpose of the hot gas duct is to conduct the high temperature helium coming out of the reactor core to the helium turbine and to feed the reactor with helium coming from the PCU Recuperator. It should be isolated in order to minimise thermal losses (improving cycle efficiency) and to limit the maximum material operating temperature.

The hot gas duct reference design – proposed by Framatome ANP Refs 1 and 2- consists of two coaxial ducts. High temperature helium flows through the inner part of the duct of minimum diameter, from the reactor to the turbine. The feed helium flows through the region limited by both the inner and outer ducts, from the recuperator to the reactor. The helium operating pressure is approximately the same in the “hot-gas side” and the “cold-gas side”. Therefore, only the outer duct is part of the pressure boundary.

The advantage of this design is that the duct conducting the high temperature helium is not part of the pressure boundary. As a result, the material of this duct, working at temperatures over 800°C, will not be subjected to the design pressure and will only be subjected to relatively small pressure differences during transient conditions. The analyses performed and reported in this document only refer to this inner duct of the hot gas duct. The outer duct is outside the scope of this study.

3. CALCULATION HYPOTHESES

3.1 REFERENCE HOT GAS DUCT

The different analyses have been carried out using a reference hot gas duct with the following geometrical characteristics (Ref. 2):

- Outside diameter of the support tube (cold duct side) $De = 1700$ mm
- Inside diameter of the liner (hot duct side) $Di = 1450$ mm
- Thickness of the support tube $Te = 25$ mm
- Thickness of the liner $Ti = 10$ mm
- Duct material \Rightarrow Alloy 1.4876 or 1.4571

3.2 MATERIAL PROPERTIES

3.2.1 Metal Parts

The different metal parts of the hot duct are made of alloy 1.4876 or 1.4571, the properties of which are similar. Table 2-1 below shows their properties at different temperatures (Ref 4):

Table 2-1

Temp (°C)	K (W/m K)	α (1/K)	C_p (J/kg K)	ρ (kg/m ³)	E (MPa)	$R_{p0.2}$ (MPa)
200	17	17 E-6	0.49	7850	186 E+9	150
400	20	18 E-6	0.52	7850	172 E+9	125
600	22.5	19 E-6	0.59	7850	155 E+9	115
850	26	19.5 E-6	0.63	7850	120 E+9	84

3.2.2 Insulating Material

A Saffil type material has been considered as insulation between the hot and cold duct sides. It is formed of ceramic fibres containing 95% Al_2O_3 .

Ref 1 gives the equivalent thermal conductivity values measured for this material with a packing density of 160 kg/m^3 in an He fluid at 40 bar. These values are shown in Table 2-2 below:

Table 2-2

Temp (°C)	400	600	800	1000
K (W/mK)	0.296	0.465	0.571	0.682

In accordance with Ref 2, a single equivalent conductivity value of 0.55 W/mK is used in the calculations.

The equivalent thermal conductivity value mainly affects the total heat transmitted in the hot duct and includes the material thermal conductivity, the convection and the radiation present during the test.

3.3 LOAD CASES CONSIDERED

In accordance with Ref 3, the maximum loads to be considered in the design of the hot duct will be based on the following events:

- Normal operating conditions \Rightarrow Conditions in accordance with section 3.3.1
- Thermal and pressure transient loads \Rightarrow Conditions in accordance with section 3.3.2

3.3.1 Normal Operating Conditions

The following are the He conditions considered on the “hot-gas” and “cold-gas” sides of the hot gas duct during normal operating conditions (Ref 2):

Hot gas side

- Helium temperature $\Rightarrow 850^{\circ}\text{C}$
- Helium pressure $\Rightarrow 70.8$ bar
- Helium mass flow $\Rightarrow 316.19$ kg/s

Cold gas side

- Helium temperature $\Rightarrow 488^{\circ}\text{C}$
- Helium pressure $\Rightarrow 71.6$ bar
- Helium mass flow $\Rightarrow 318.2$ kg/s

3.3.2 Thermal and Pressure Transient Loads

According to Ref. 3, the maximum transient loads to be considered are:

- Maximum temperature gradient of cold gas side He $\Rightarrow \Delta T = -23^{\circ}\text{C/s}$ for 8.83 s, starting from the operating conditions
- Maximum pressure gradient of cold gas side He $\Rightarrow \partial P = 1.0$ MPa/s for 7 s, starting from the operating conditions.

3.4 PRESSURE DROP IN THERMAL INSULATION

The hot duct pressure drop events will start a process to remove the He stored in the space occupied by the thermal insulation. It must be borne in mind that the thermal insulation occupies less than 10% of the total volume, so the remaining volume will therefore be occupied by He.

To evaluate the pressure differences between the hot gas side (thermal insulation chamber) and the cold gas side He, the pressure drop which will take place in the thermal insulation during a pressure drop event must be estimated.

This pressure drop is estimated on the basis of Ref 5 which gives the following values for pressure drop in air at 1 bar for each metre length of insulation:

- Compacted fibres $\Rightarrow \Delta P \text{ (N/m}^2\text{)} \approx 680 V^{1.097}$ ($V \Rightarrow$ Velocity of the air m/s)
- Tissues or wrapped fibres $\Rightarrow \Delta P \text{ (N/m}^2\text{)} \approx 600 V^{1.155}$ ($V \Rightarrow$ m/s)

These pressure drop values have been compared to the pressure drop values provided by the manufacturers of glass fibre materials used in filters and the results were similar to those obtained with the formulae.

These are only approximate values as there will be different factors to take into account, such as the extent to which the insulating material is compacted. In any event, we shall consider these pressure drop values to be multiplied by an increase coefficient of four (4) in order to perform conservative pressure drop calculations.

To extrapolate the values of pressure drop in air to values of pressure drop in He at pressures other than 1 bar and different temperature values, we shall consider a pressure drop value multiplied by the ratio of densities between the He and the air ($\approx 1 \text{ kg/m}^3$).

3.5 He VELOCITY DURING PRESSURE DROP

The hot duct pressure drop events will start a process to remove the He stored in the space occupied by the thermal insulation. The following formula has been used to evaluate the velocity of He discharge during these events:

$$\frac{P_1}{P_2} = \left(\frac{d_1}{d_2} \right)^k \quad \frac{T_1}{T_2} = \left(\frac{d_1}{d_2} \right)^{k-1} \quad \frac{P_2}{d_2^k} = C$$

where:

- Point (1) is the initial state and point (2) is a state during the pressure drop event
- $P_{1,2} \Rightarrow$ pressure
- $T_{1,2} \Rightarrow$ temperature
- $d_{1,2} \Rightarrow$ density
- $K = 1.666$ (C_p/C_v of the He)

If during the pressure drop event we consider the following calculation data:

- Variation in pressure over time $\Rightarrow \partial P \equiv \frac{\Delta P}{\Delta t}$ (Pa/s)
- Flow area in He discharge $\Rightarrow A_s$ (m²)
- Volume of He enclosed in the isolation chamber $\Rightarrow V_o$ (m³)
- He discharge flow $\Rightarrow q_2$ (kg/s)

With these data, the He discharge velocity (V_2) as it passes through the flow area A_s is calculated as follows:

$$\frac{\partial d_2}{\partial t} = \frac{\partial P}{C \times K \times d_2^{K-1}} \quad q_2 = \frac{\partial d_2}{\partial t} V_o \quad A_s \times V_2 = \frac{q_2}{d_2}$$

$$V_2 = \frac{V_o}{A_s} \frac{\partial P}{K \times P_2}$$

4. CONNECTING SPACERS BETWEEN SUPPORT TUBE AND LINER

4.1 GEOMETRICAL CONFIGURATIONS STUDIED

To connect the support tube structure and the liner, a metal spacer is installed which ensures that:

- The thermal dilations between the external support tube and the liner are compatible, so that the stresses on the connection are as low as possible
- A solid stiff connection is established between the external support tube and the liner

Three types of connecting spacers have been studied, as defined in Figures A, B and C of Appendix A. The geometrical and manufacturing characteristics of each of the connecting spacers are described below.

4.1.1 Type A — V-shaped Spacer (Reference Design)

- 4 mm-thick metal plate, forming a single V-shape part
- Each of these spacers is machine form forged. The machined part includes part of the support tube and the liner
- The dimensions considered are shown in Figure A of Appendix A

4.1.2 Type B — 2L-shaped Spacers

- Formed by a 5 mm thick cylindrical plate. This plate is connected to the liner by means of a 10 mm thick perpendicular plate and to the support tube by means of an 8 mm thick perpendicular plate
- The three plates which comprise the spacer are manufactured from cut plates which are welded together
- The spacer is connected to the liner and the support tube by means of welds
- The dimensions considered are shown in Figure B of Appendix A

4.1.3 Type C — LCL-shaped Spacer

- Formed by two 5 mm and 8 mm thick cylindrical plates. These plates are connected to the liner by means of a 10 mm thick perpendicular plate and to the support tube by means of an 5 mm thick perpendicular plate
- The plates which comprise the spacer are manufactured from cut plates which are welded together
- The spacer is connected to the liner and the support tube by means of welds
- The dimensions considered are shown in Figure C of Appendix A

4.2 THERMAL STRESSES ON THE SPACERS

4.2.1 Stress States in Normal Operating Conditions

Three types of spacers for a hot duct configuration have been analysed defined by the following:

- Geometry of the support tube and liner in accordance with the data given in section 3.1
- Thermal conductivity of the insulation between the support tube and liner in accordance with section 3.2.2
- Temperature of 488°C considered on the external face of the support tube in accordance with section 3.3.1
- Temperature of 850°C considered on the internal face of the liner in accordance with section 3.3.1

A finite element model has been built of each of the three types of spacers and thermo-mechanical analyses have been performed to obtain the maximum stress states on the spacers. The finite element models are illustrated in Figures 1, 4 and 7 of Appendix B.

The maximum stress and temperature values obtained on the three types of spacers are given in Table 3-1 below.

Table 3-1

	Point	Type A	Type B	Type C
1	S (MPa)	353	370	382
	T (°C)	550	550	550
2	S (MPa)	290	240	250
	T (°C)	620	750	750
3	S (MPa)	200	100	170
	T (°C)	820	820	820

Figures 2, 5 and 8 of Appendix B show the temperature distribution in each one of the three spacer configurations. Figures 3, 6 and 9 show the stress distribution in each one of the three spacer configurations.

Analyses of other geometrical configurations have been carried out and the following results obtained:

- Double-A configuration (Figure 10, Appendix B) ⇒ The resulting stress state is similar to that obtained with the Type A configuration
- Double-C configuration (Figure 11, Appendix B) ⇒ The resulting stress state is similar to that obtained with the Type C configuration
- Configuration Type B, with curved ends (Figure 12, Appendix B) ⇒ The stress state obtained in this configuration is more critical than that in configuration Type B

The following conclusions can be derived from the stress analyses carried out for normal operating conditions:

- Considering a maximum allowable secondary stress limit of $2 \times R_{p02}$, the stress states obtained at different temperatures are higher than these maximum value
- This means that the material will suffer slight permanent/plastic deformations which will accumulate with the hot duct thermal cycles
- The maximum allowable number of thermal cycles subject to fatigue for this stress level can be estimated as $n > 10^5$ cycles, in accordance with ASME III Division 1-NH (Figure T-1420-1B)

- Since the allowable number of thermal cycles subjected to fatigue $n > 10^5$ is far greater than the foreseen startup and shutdown number of cycles during the plant lifetime, it is considered that no cracks will appear in the different metal parts of the hot duct due to material fatigue

4.2.2 Stress States during Thermal Transients

Stress analyses have been carried out for the most unfavourable thermal transient load case, indicated in section 3.3.2. The following have been considered in these transient analyses:

- Variation in the external He temperature of $\Delta T = -23^\circ\text{C/s}$ (hot side) for ≈ 9 s. At the end of the transient, the He temperatures considered are $\approx 650^\circ\text{C}$ on the hot side and $\approx 375^\circ\text{C}$ on the cold side
- It has been considered that the He flow is maintained during the thermal transient, imposing He-wall heat exchange coefficients of $\approx 1500 \text{ W/m}^2\text{K}$ in the hot duct and $\approx 1300 \text{ W/m}^2\text{K}$ in the cold duct
- A thermal transient of 310 s was analysed so that after the first 9 s the external He temperature is kept constant, both on the hot side and the cold side

The analyses of the thermal transients for the different hot duct configurations A, B and C produced similar results:

- During the ≈ 9 s thermal transient, the following wall temperature variation values were produced: liner $850^\circ\text{C} \Rightarrow \approx 845^\circ\text{C}$; support tube $488^\circ\text{C} \Rightarrow \approx 460^\circ\text{C}$
- A period of time in excess of 300 s is required to raise the temperature of the pipe walls to a temperature close to that of the external He
- The maximum stress states on the metal connecting part are obtained approximately 200 s after the transient begins. The maximum stress states reached in the cold part of the connecting spacers increase by approximately 75-80% with respect to the stresses in normal operating conditions. The maximum stresses on the hot part of the connecting spacers are maintained approximately the same as the values obtained for normal operating conditions

The maximum stress states reached during thermal transients for the three types of spacers is $S \approx 650 \text{ MPa}$ at a maximum temperature of about 550°C .

This thermal stress state is more critical than that obtained during normal operating conditions. Therefore the accumulated deformation in the metal spacer would increase with these types of events.

Taking into account that the connecting spacer is axisymmetrical, the deformation and the thermal loads are also axisymmetrical. The deformation will practically have no effect on either the liner or the support tube because the stress states on these components are lower than the maximum values obtained.

The maximum allowable number of thermal cycles subject to fatigue for these levels of maximum stresses and temperatures obtained in the thermal transients can be estimated as $n > 500 - 1000$ cycles, in accordance with ASME III Division 1-NH (Figure T-1420-1B).

If the number of cycles (n) is exceeded, small fissures may appear in the metal connecting part. This will not cause any significant problems, as long as the cracks are not big enough to considerably diminish the stiffness provided by the metal connecting spacer.

4.3 STRUCTURAL STIFFNESS OF THE SPACERS

The stiffness of each of the different types of connecting spacers have been analysed.

The stiffness is calculated under the following conditions:

- The radial displacement of the external face of the support tube is restricted
- To obtain the radial stiffness, a unit radial displacement is introduced into the liner and the axial displacement is restricted. The radial reaction between the liner and the metal spacer is obtained
- To obtain the axial stiffness, a unit axial displacement is introduced into the liner and the radial displacement is restricted. The axial reaction between the liner and the metal spacer is obtained

The following are the stiffness results obtained for the three types of connecting spacer analysed:

Stiffness	Type A	Type B	Type C
Radial (N/m)	2.8 E+9	7.3 E+9	8.1 E+9
Axial (N/m)	3.0 E+9	5.0 E+9	2.5 E+9

If we take the axial stiffness of the duct as the most representative stiffness, we can see that a Type B connection is practically equivalent to the double-A or double-C type connections.

4.4 HEAT TRANSFERRED THROUGH THE INSULATION

An analysis has been carried out of the heat transmitted through the insulating wall (thermal losses) between the liner and the external support tube, based on the following calculation conditions:

- Temperature of the external face of the support tube \Rightarrow 488°C
- Temperature of the internal face of the liner \Rightarrow 850°C
- Thermal conductivity of the insulation $K = 0.55$ W/mK
- Conductivity of the metal parts \Rightarrow see section 3.2

The analysis of the heat transferred has been carried out for a meter length hot gas duct, with the metal spacer centred in that portion of the duct. The results of the heat transferred for each of the different types of spacers are provided in the following table:

Type A	Type B	Type C	Type Double A	Type Double C
10.3 kW/m	12.0 kW/m	11.8 kW/m	11.0 kW/m	—

It can be seen that Type B spacers transmit 16% more heat than Type A spacers and 10% more than double-A type spacers.

4.5 CONCLUSIONS FOR THE DESIGN OF THE SPACERS

The following conclusions can be derived from the analyses of the different types of metal connection spacers between the support tube and the liner:

- From the manufacturing point of view, the Type A connection requires machining of the metal connecting parts. On the other hand, connection Types B and C would be formed by cut plates welded together and in turn welded to the support tube and the liner
- From the point of view of maximum thermal stresses, the three types of connections give similar stress results
- For spacer Types B and C, the stress states on the connections with the support tube and the liner are low, which means it would be acceptable to weld them together
- From the point of view of stiffness, the Type B connection is the stiffest, being equivalent to a double-A or double-C type connection
- From the point of view of heat transferred through the insulating wall (thermal losses), the Type A connection gives better thermal insulation compared to the other types of connections

5. FIBRE FILTERING DURING PRESSURE DROP

5.1 GEOMETRICAL CONFIGURATIONS OF FILTERS STUDIED

Sudden external He pressure drop events can give rise to the entrainment of insulation fibres from the thermal insulation chamber into the hot duct. To prevent this, a filter system shall be installed which guarantees that:

- The thermal dilations between the external support tube and the liner are compatible, so that the stresses on the connecting part are as low as possible
- Insulation fibres are prevented from getting inside the hot duct

Two types of filters have been studied and are defined in Figures D and E of Appendix A. The geometrical manufacturing characteristics of each of the filters are described below.

5.1.1 Type A Filter — (Reference Design, Ref 2), Figure D, Appendix A

- The thermal insulation is separated from the liner by a 5 mm thick, perforated internal pipe which is welded to a machined part installed in the liner
- Axial thermal deformation is made compatible by allowing the axial dilation of the 5 mm pipe in a contact area between the two pipe sections (see Figure D, Appendix A). Given the high temperatures (850°C) of this contact area, it requires very precise machining and surface treatment
- To prevent the entry of fibres in the helium flow, a closed chamber is created between the liner and the 5 mm perforated pipe. This chamber is sealed by machined ceramic rings which are connected to the 5 mm pipe and are in contact with the liner pipe
- The chamber is approximately 20 mm thick and reduces the space occupied by the thermal insulation. A comparison of filter Type A with filter Type B shows that filter Type A will transfer approximately 20% more heat through the hot duct than filter Type B

5.1.2 Type B Filter — Ring-type Filter, Figure E, Appendix A

- The filter is manufactured in the form of a ring, as a part independent of the hot duct. This filter comprises the following parts:

- 5 mm perforated internal and external pipes
 - 2 lateral, cut plates on which the perforated pipes are mounted and welded. The filter is installed between the two 5 mm perforated pipes
 - Filter formed by wrapped fibre insulation arranged circumferentially and compacted. The filter fibre is separated from the 5 mm perforated pipes by means of metal wire mesh
- The ring-type filter is installed in the hot duct by means of two lateral L-shaped profiles welded to the liner. The joint is made using a flexible temperature-resistant material and screws with axially elongated holes for thermal dilation. Once the screws have been inserted they can be spot welded

5.2 PRESSURE DROP IN THE INSULATING CHAMBER

5.2.1 Type A Filter (Reference Design, Ref. 2)

During He pressure drop events with this type of filter, the maximum pressure drop between the He of the internal thermal insulation chamber and the external He is produced in the gap section located in the contact between the ceramic rings and the liner. The pressure drop in the thermal insulation is considered negligible (see pressure drop with Type B filter).

A finite model was built of a hot duct section with a Type A filter (see Figure 13, Appendix B). Analyses were carried out with this model and the following results obtained:

- If it is assumed that the ceramic rings make contact with the liner before the hot duct is heated to operating temperatures, when these temperatures are reached the liner is displaced in radial direction to a value 5 mm more than that of the ceramic rings due to the different thermal expansion coefficients. Both parts will continue to be in contact and there will be a radial compression force of $F_r = 8E+5$ N/m between each of the ceramic rings and the liner
- A higher pressure inside the thermal insulation chamber with respect to the cold gas side He (between 1 and 7 MPa) will not cause any significant relative opening between the rings and the liner, especially the outer ceramic ring, which is the ring that retains the pressure

Therefore, assuming contact between the rings and the liner, the cold gas side He pressure drop events will not cause any opening between the ceramic rings and the

liner. The thermal insulation chamber could therefore become overpressurised and give rise to unallowable stress states.

Therefore, in order to control the pressure drop process in the insulating chamber, it must be ensured that there is a discharge opening between the ceramic rings and the liner during hot duct operating conditions and during the different thermal transients.

This required discharge opening will have to be calculated to obtain the desired differential pressure in the insulating chamber with respect to outside pressure, so as to produce acceptable stress states.

5.2.2 Type B Filter

To calculate the pressure drop inside the thermal insulation during He pressure drop events in accordance with section 3.4, the following values were used:

- Variation in maximum pressure $\Rightarrow \partial P = 1.0 \text{ MPa/s}$
- Volume of He enclosed between the two spacers $\Rightarrow V_0 \cong 0.7 \text{ m}^3$, considering a distance of $\cong 1.6 \text{ m}$ between spacers
- Minimum He flow area $\Rightarrow A_s \cong 0.2 \text{ m}^2$, section between the filter and the wall of the support tube. A length of $L_p \approx 0.2 \text{ m}$ is conservatively considered as maximum length with a minimum flow area section (A_s)

If we assume that the pressure drop ∂P occurs from normal operating conditions $\Rightarrow P_1 = 7.2 \text{ MPa}$; $T_1 = 850^\circ\text{C}$; $d_1 = 3 \text{ kg/m}^3$, in accordance with section 3.5 the maximum velocity reached by the He in the section A_s will be $V_2 = 0.3 \text{ m/s}$. In accordance with section 3.4 the pressure drop value in the section A_s for an insulation material length L_p can be estimated as:

$$\Delta P \approx 4 \times L_p \times d_1 \times 680 \times V_2^{1.097} = 0.435 \text{ E-3 MPa}$$

If we assume that the pressure drop ∂P occurs in low pressure operating conditions $\Rightarrow P_1 = 2.0 \text{ MPa}$; $T_1 = 500^\circ\text{C}$; $d_1 = 1.2 \text{ kg/m}^3$, in accordance with section 3.5 the maximum velocity reached by the He in the section A_s is $V_2 = 1.0 \text{ m/s}$. In accordance with section 3.4 the pressure drop value in the section A_s for an insulation material length L_p can be estimated as:

$$\Delta P \approx 4 \times L_p \times d_1 \times 680 \times V_2^{1.097} = 0.787 \text{ E-3 MPa}$$

A similar pressure drop value would be obtained in the fabric insulation (see section 3.4).

As may be seen, the pressure drop value in the insulation can be considered insignificant compared to the value ∂P . It can therefore be ensured that the pressure inside the insulating chamber will be practically the same as the pressure of the cold side gas He during pressure drop events.

5.3 STRESSES ON THE FILTER STRUCTURE

5.3.1 Type A Filter (Ref. 2)

If the joint between the ceramic rings and the 5 mm perforated pipe which supports them is rigid, very high stress states will occur in the ceramic rings due to the different thermal expansion coefficients between the steel and the ceramic material.

The ceramic rings should therefore be connected to the 5 mm pipe in such a way that the joint is not rigid, allowing a different radial displacement between the two components. It would be recommendable that the rings were not continuous, but rather that they were assembled in segments so that dilation of the ceramic material would not produce circumferential stresses.

5.3.2 Type B Filter

The filter is manufactured in the form of a ring, as a part independent of the hot duct.

The fibre fabric which serves as a filter is enclosed within the structure of two metal perforated pipes, which ensures that the filter wrapped fibre will not suffer relative axial displacements due to axial dilation of the hot duct.

The external metal perforated pipe of the filter will reach a temperature different to that of the internal perforated pipe which will generate a stress state between the two pipes. These thermal stress values can be very conservatively estimated as follows:

$$s = \frac{850 - 488}{2} \times E \times a \times \frac{1}{2} \cong 275 \text{ MPa}$$

This secondary stress state could cause the material to suffer slight deformations which will accumulate during the startup and shutdown cycles, but they are far from the stress states that can cause cracks due to material fatigue.

The ring-type filter is installed in the hot duct by means of two lateral L-shaped profiles welded to the liner. The joint is made using a flexible temperature-resistant material and screws with axially elongated holes for thermal dilation.

The use of flexible joints between the filter and the connecting part to the liner allows different radial displacements of the liner and the filter structure so that stress states are not generated due to these relative displacements. In addition, these joints must prevent the entrainment of insulation fibres through the joints during He pressure drop events.

6. CONCLUSIONS

Based on the hot gas duct reference design (Ref. 2), thermomechanical calculations have been carried out for the both the normal operating conditions and transients. In particular, the design of the connecting spacers and the behaviour of the thermal insulation was analysed.

Connecting spacers:

Three types of connecting spacers have been analysed (A, B and C), which are defined in Figures A, B and C of Appendix A. Type A being the reference design (Ref. 2).

From the point of view of manufacturing and assembly, spacer Types B and C do not require any kind of special machining and can be welded directly to the support tube and the liner.

From the point of view of mechanical stiffness, spacer Type B is the most rigid with a stiffness comparable to a double-A type spacer or a double-C type spacer.

The maximum stress state on the spacers is reached during the thermal transient event analysed, which gave stress states of the order of 75-80% greater than those in normal operating conditions. This maximum stress state is reached approximately 200 s after initiation of the event.

The maximum stress states can reach values which give rise to cracks in the spacer due to metal fatigue, based on a number of thermal transient cycles of the order of $n \cong 500 - 1000$ cycles.

Regarding the heat transferred through the insulation, Type A has better thermal insulation with 10.3 Kw/m of thermal losses.

Fibre filtering:

Two types of filters (A and B) have been studied, as defined in Figures D and E of Appendix A, filter type A being the reference design.

From the point of view of manufacturing and assembly, filter Type B is made as an independent part which is mounted on the liner structure and joined to it by sealed, flexible joints and screwed to parts with elongated holes so that the joint is not subjected to thermally induced forces.

During external He pressure drop events, with the Type B filter there will be no significant differential pressure between the insulating chamber and the external He. With the Type A filter, the differential pressure in the insulating chamber could be significant and it would be necessary to control this pressure drop by ensuring some depressurisation openings.

7. REFERENCES

1. ZFY16-400636724, *Final Report*, Framatome ANP
2. ZFY16-0600191597, *Intermediate Report*, Framatome ANP
3. 092-110-CE-SV-EA-03/0007, *Hot Duct Transient Operating Conditions*
4. ASME III, Parts A, B and C, 1998 Edition
5. *Handbook of Hydraulic Resistance*. 3rd Edition

APPENDIX A
FIGURES

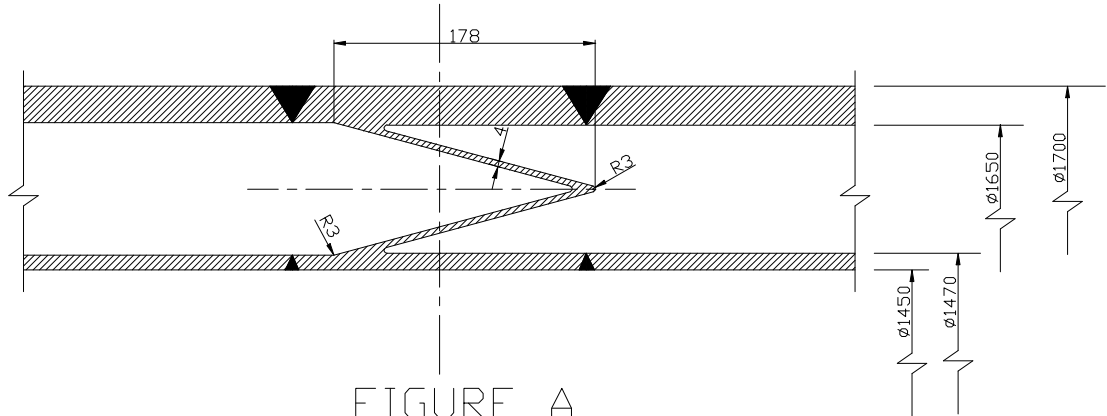


FIGURE A
(TYPE A SPACER)

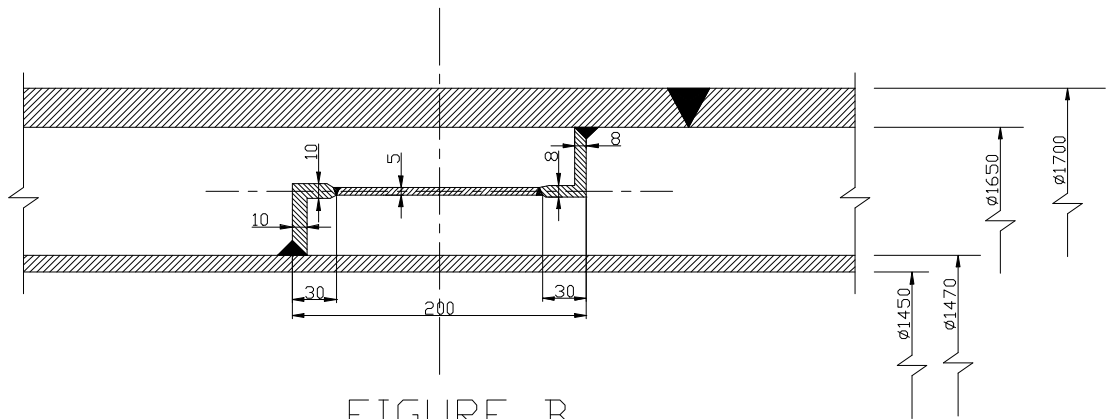


FIGURE B
(TYPE B SPACER)

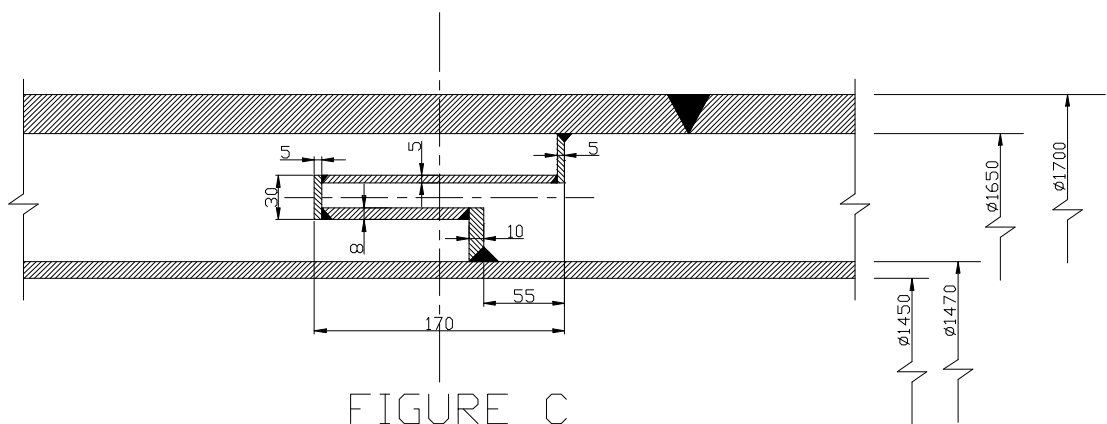


FIGURE C
(TYPE C SPACER)

00-Y-X-10302-F3/ Issue 1

00-Y-X-10302-F3/ Issue 1

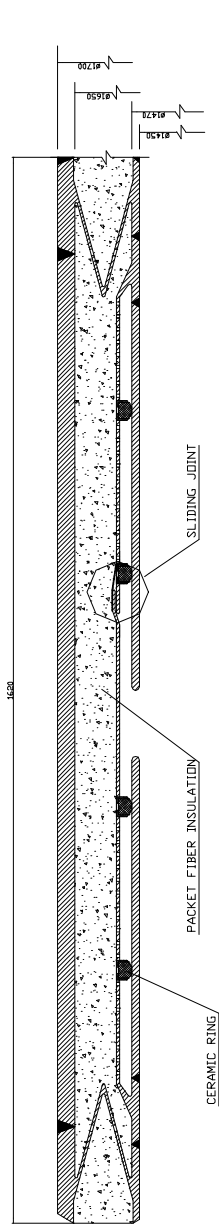


FIGURE D
(TYPE A FILTER)

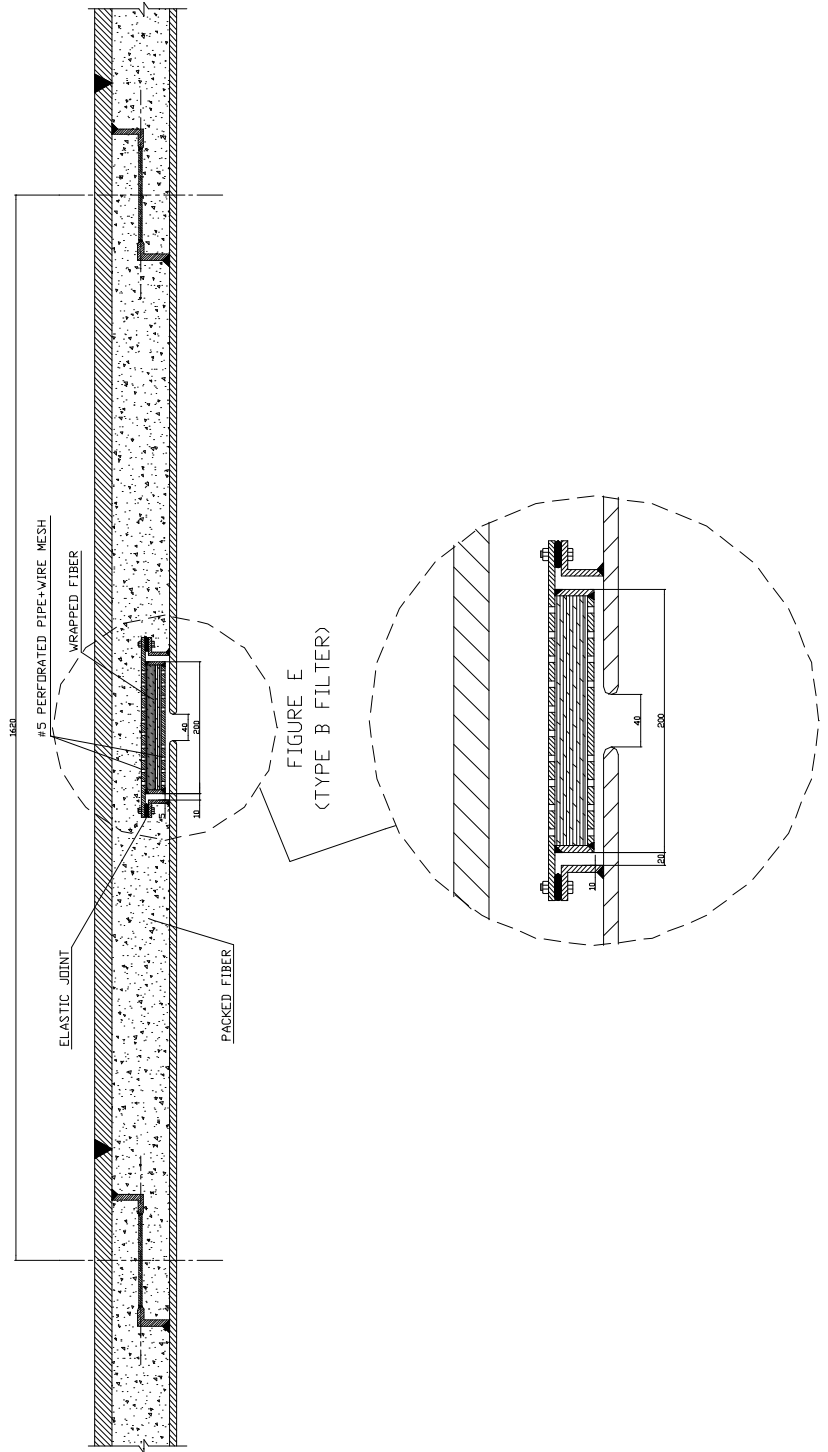
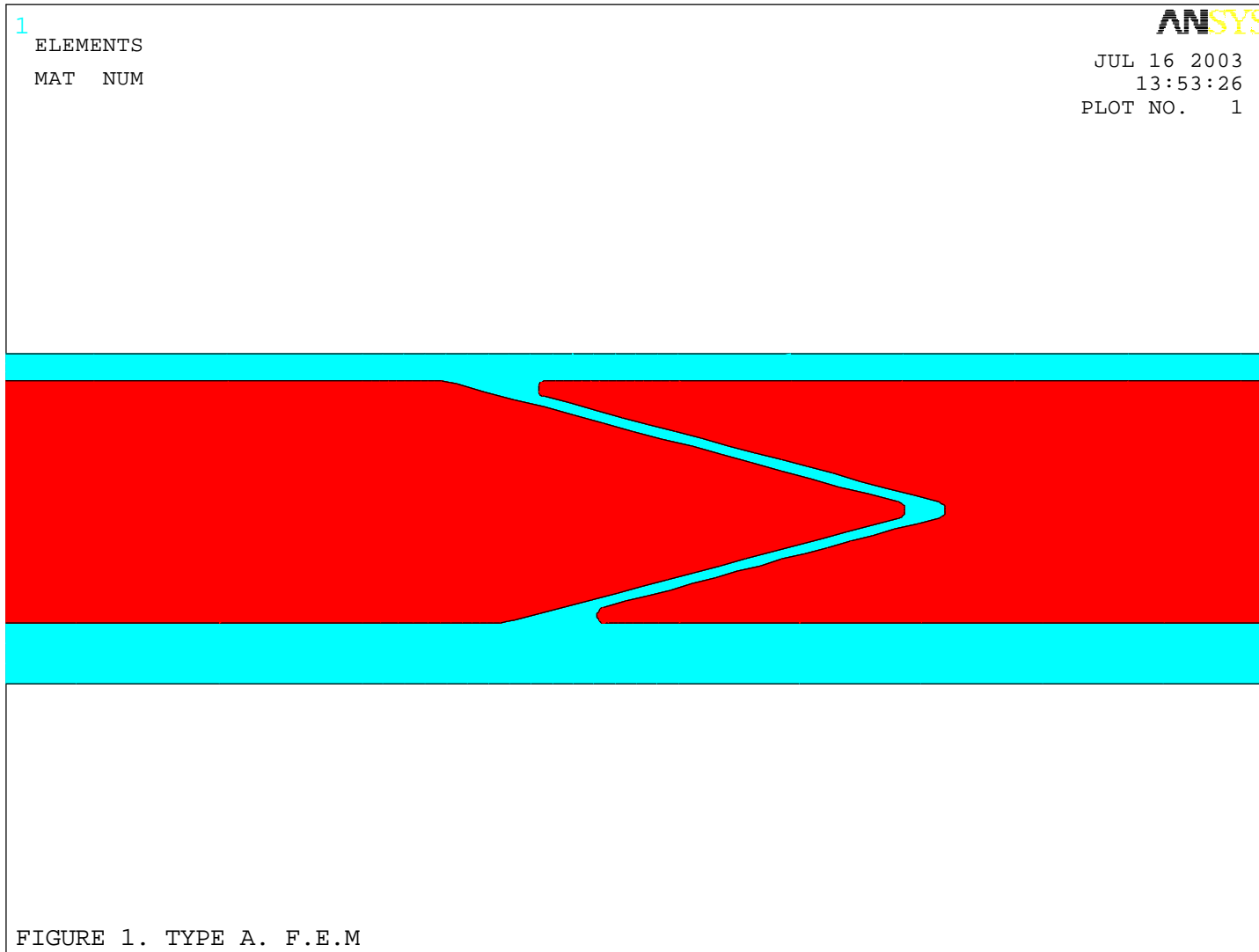
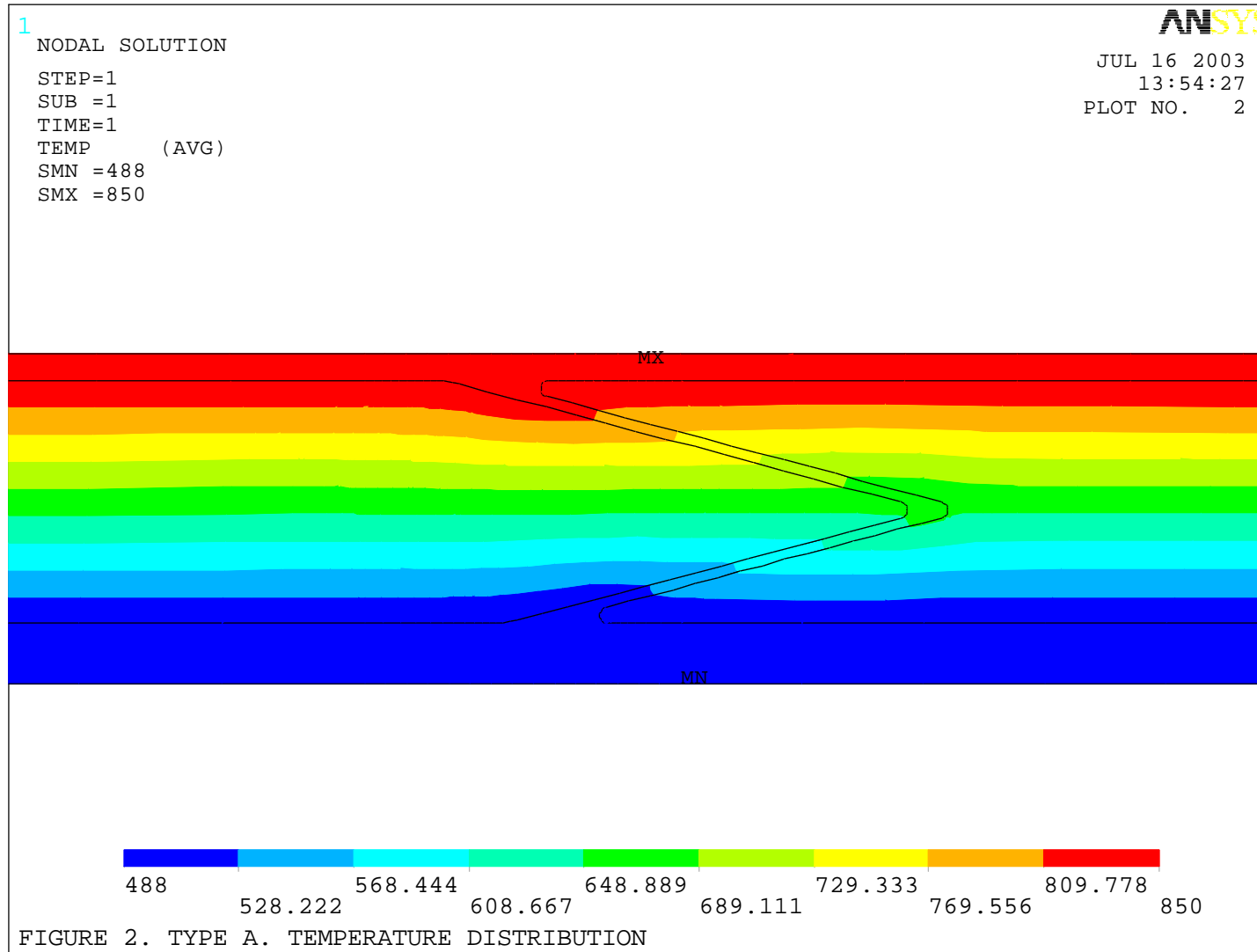


FIGURE E
(TYPE B FILTER)

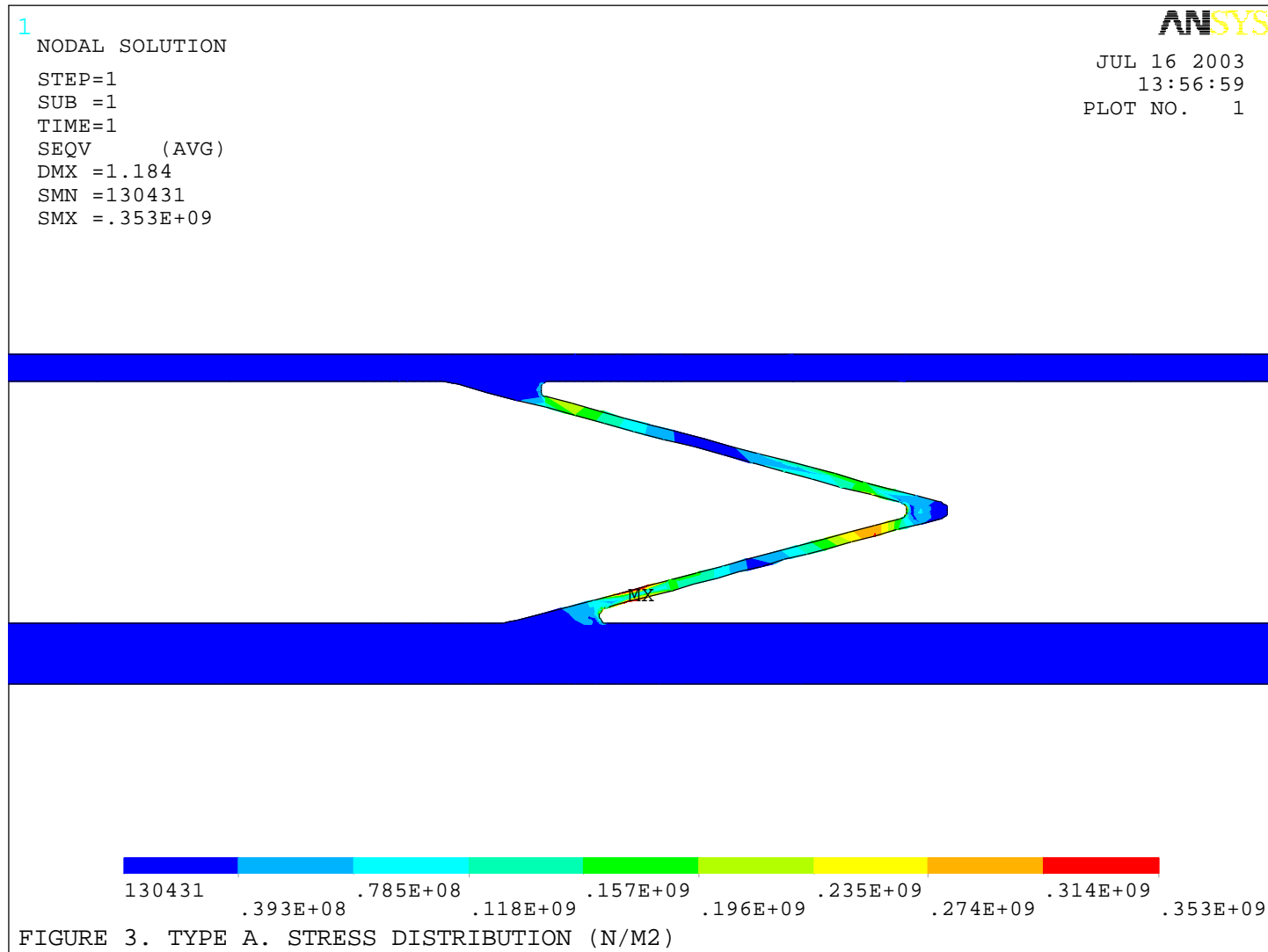
APPENDIX B

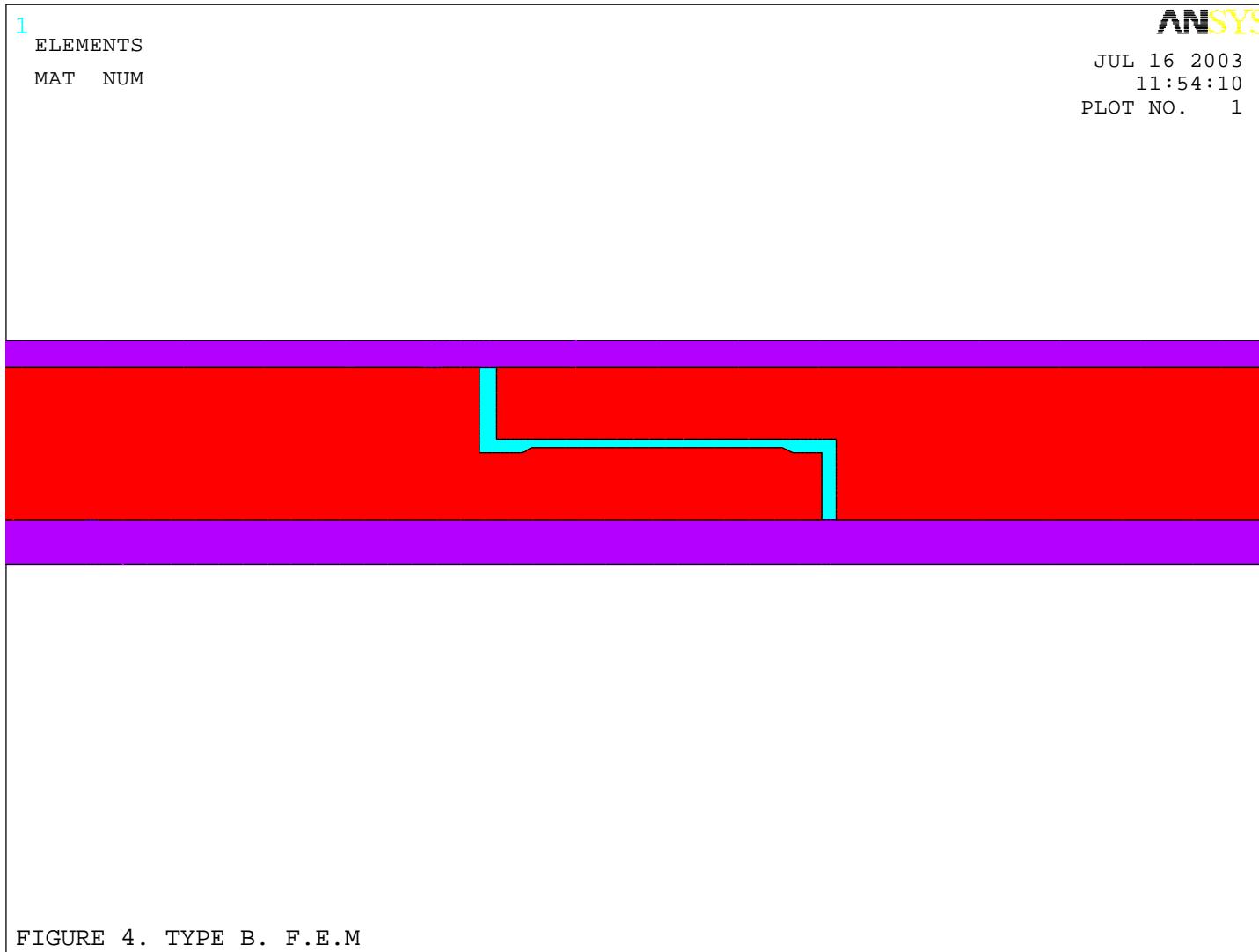
F.E.M FIGURES



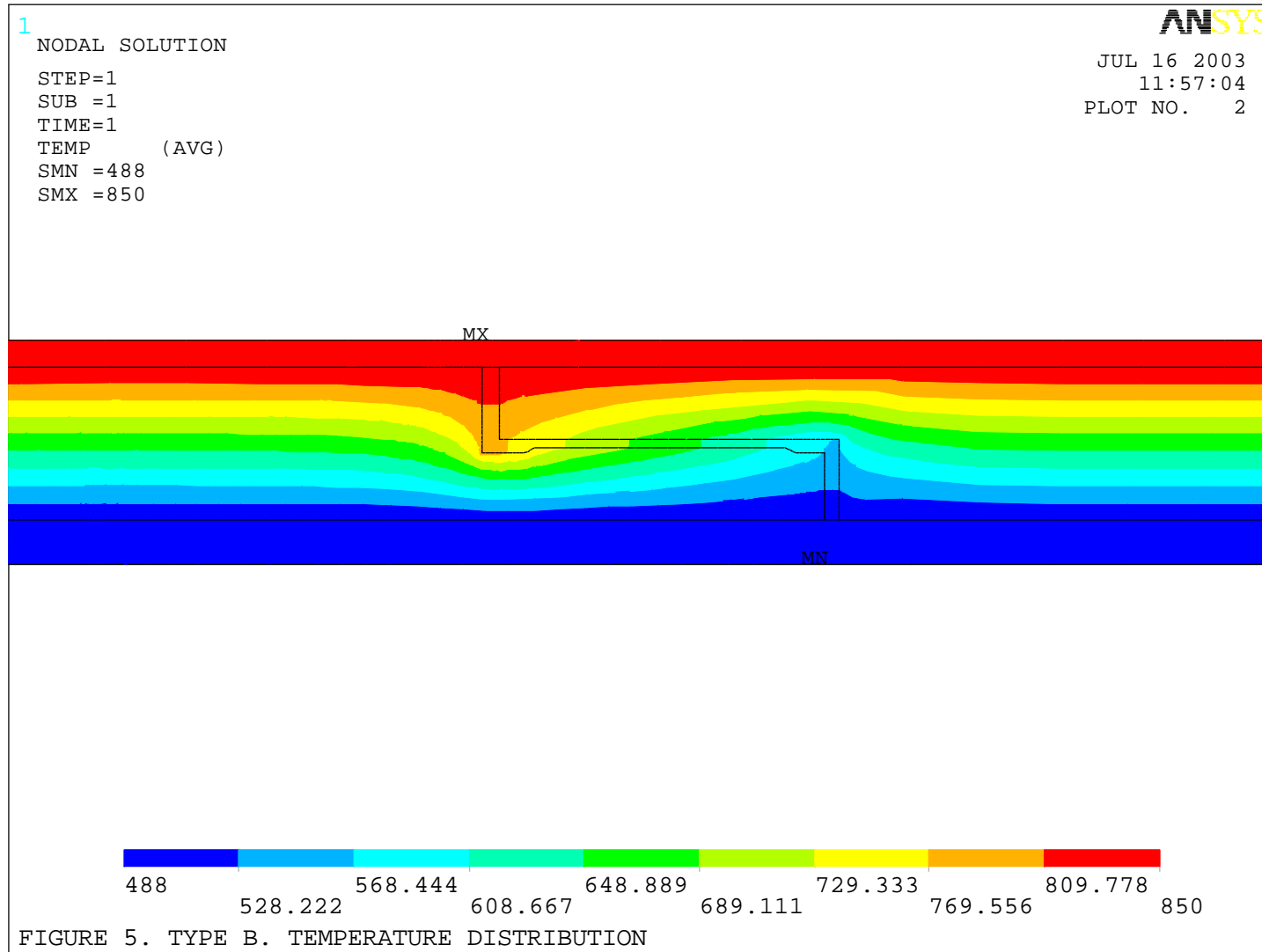


00048539

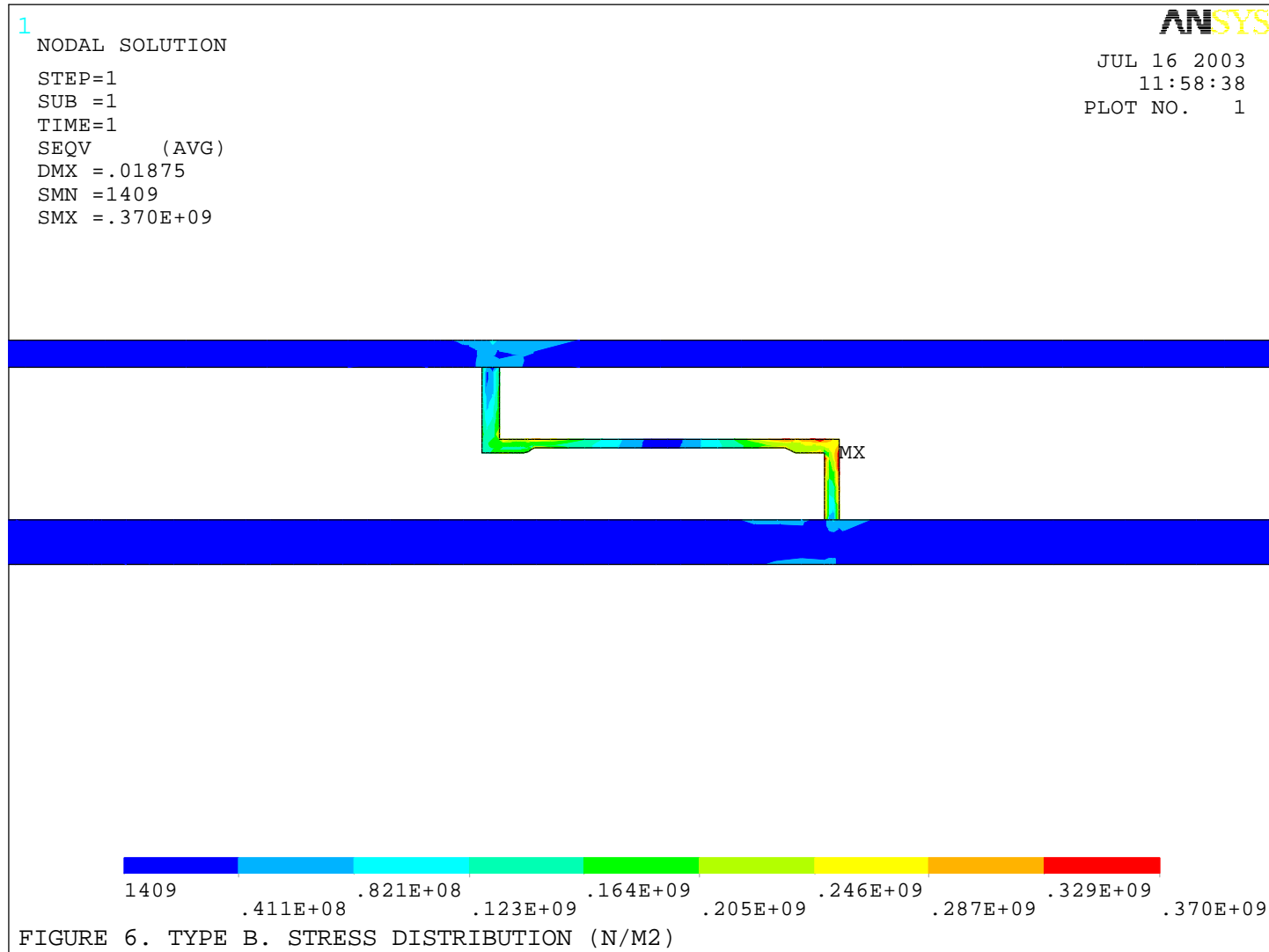




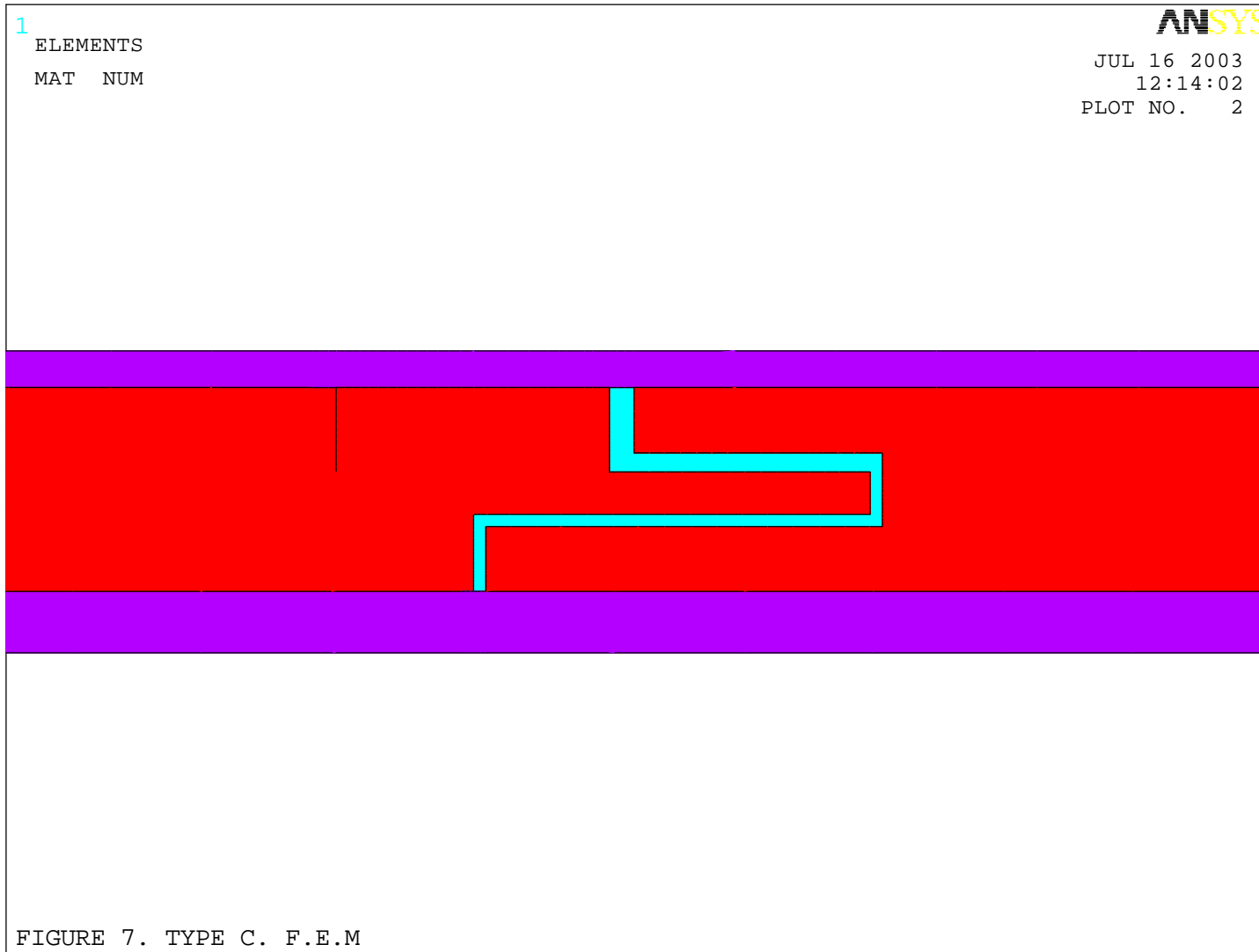
00048539

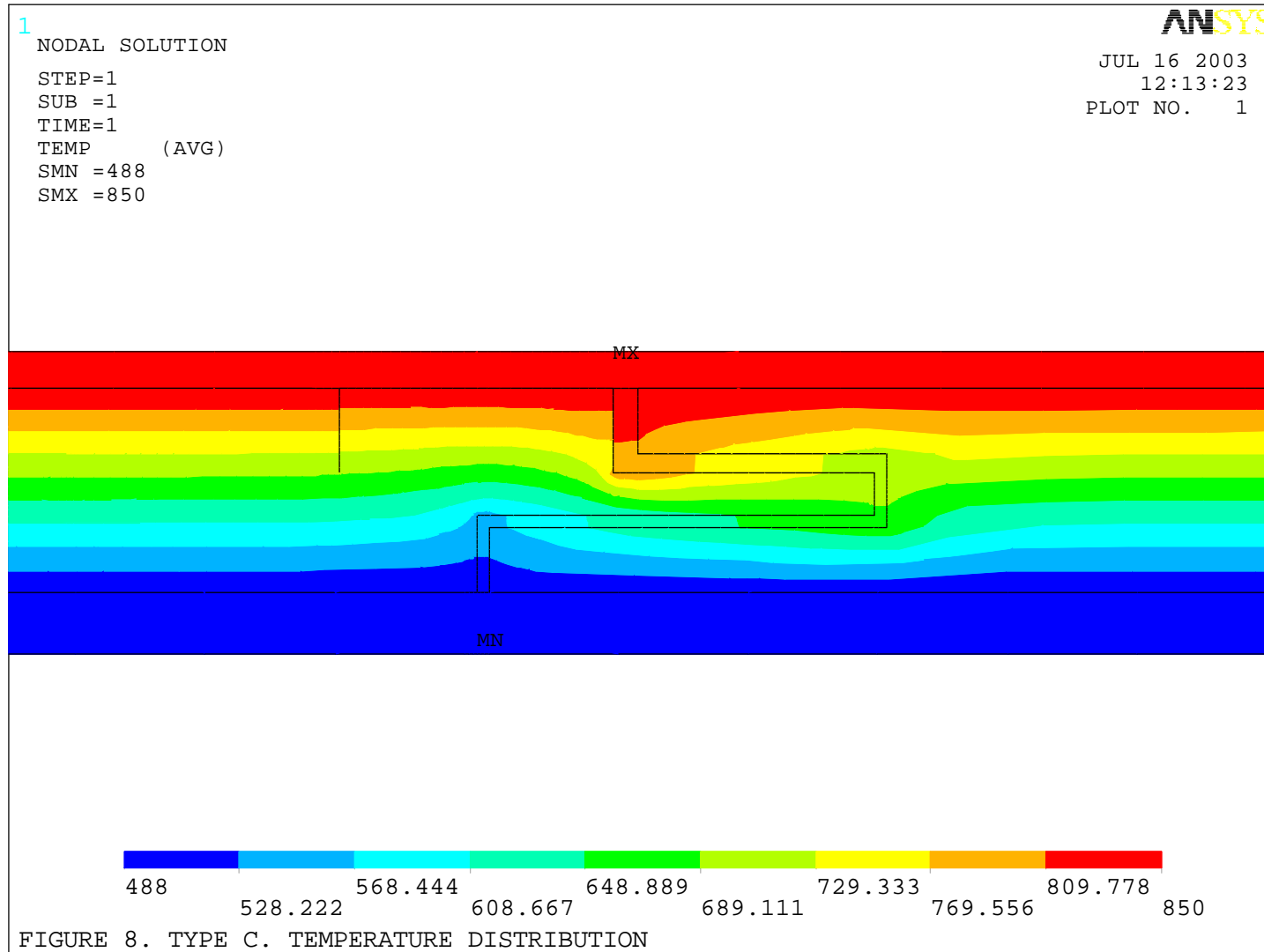


00048539

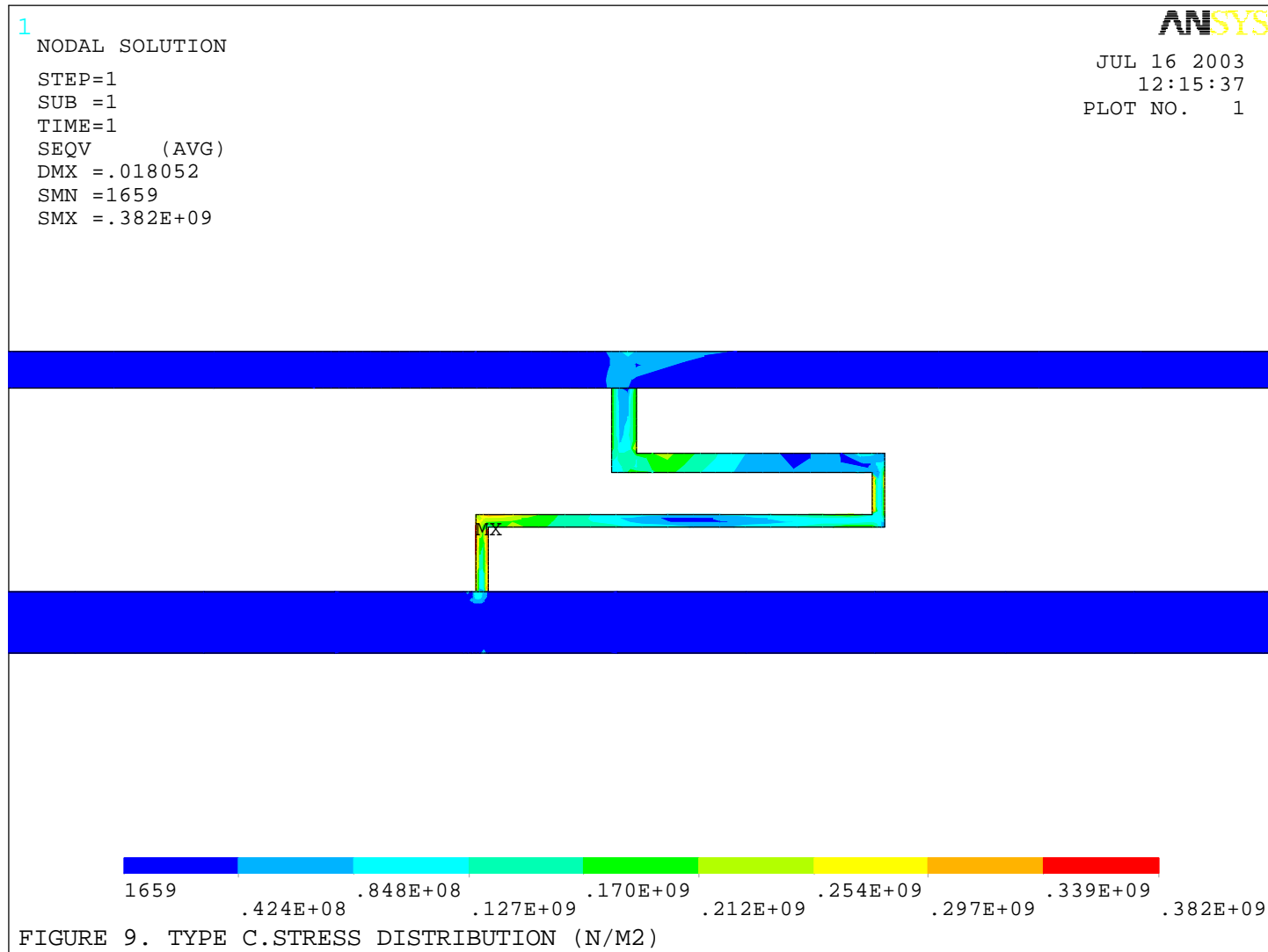


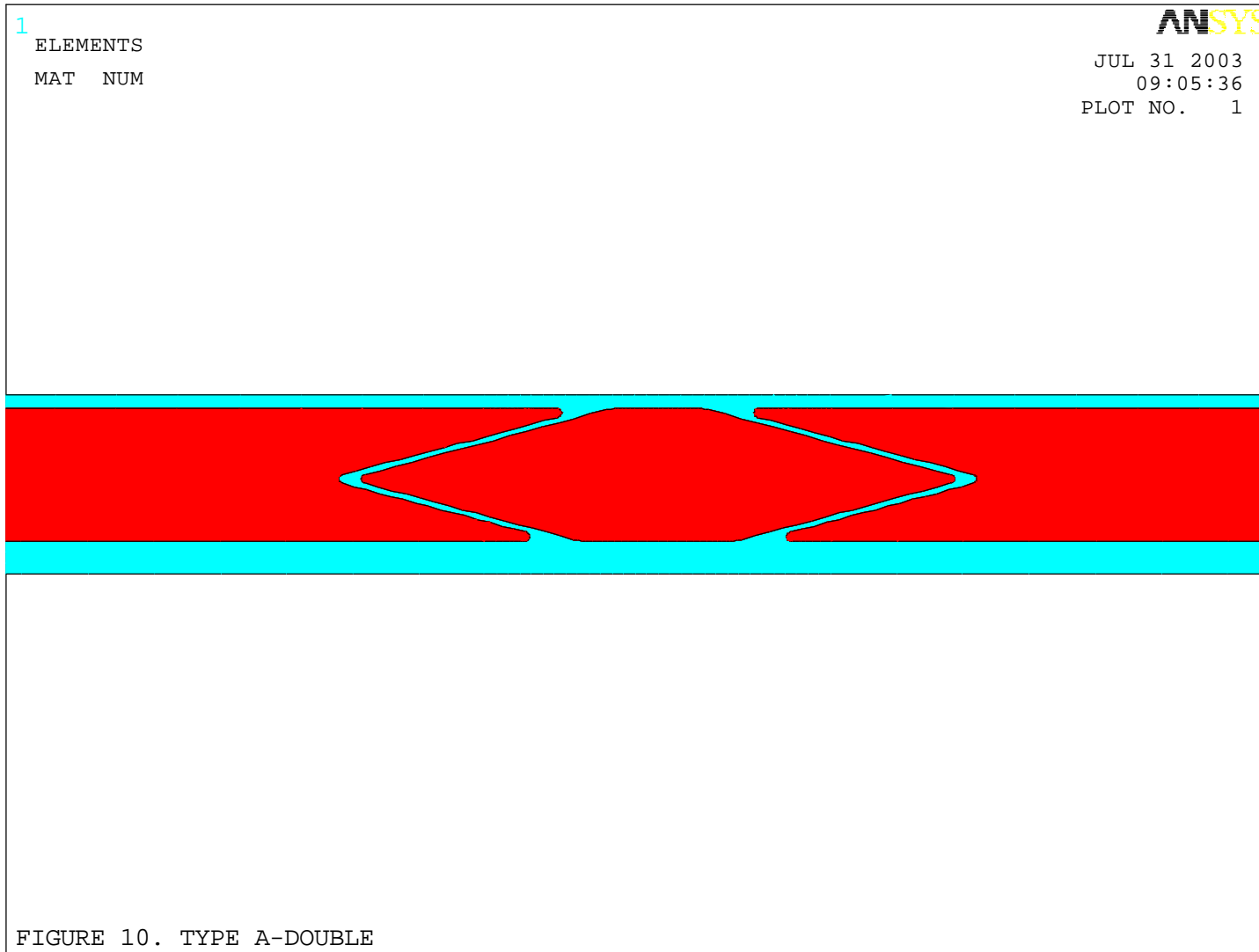
00048539

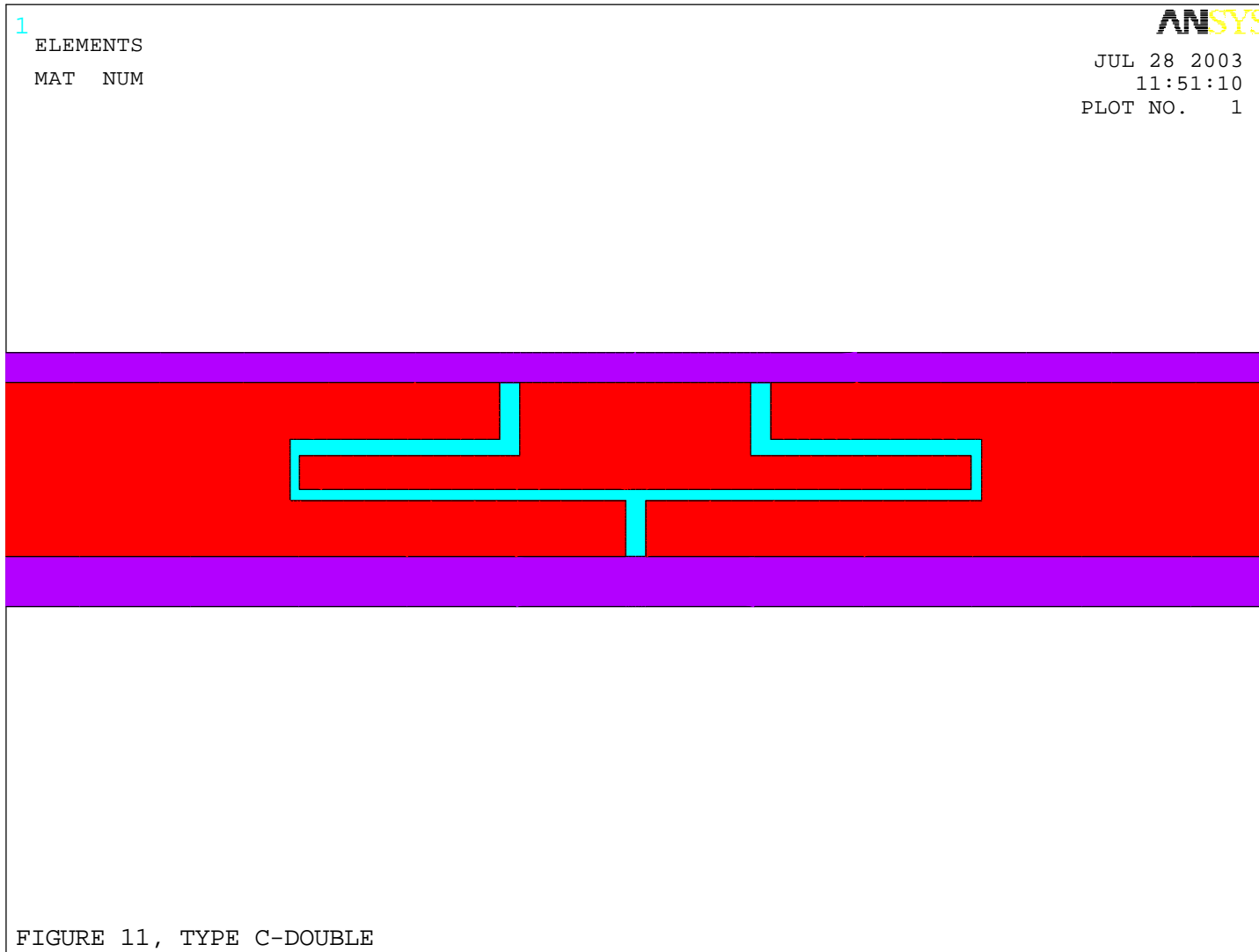




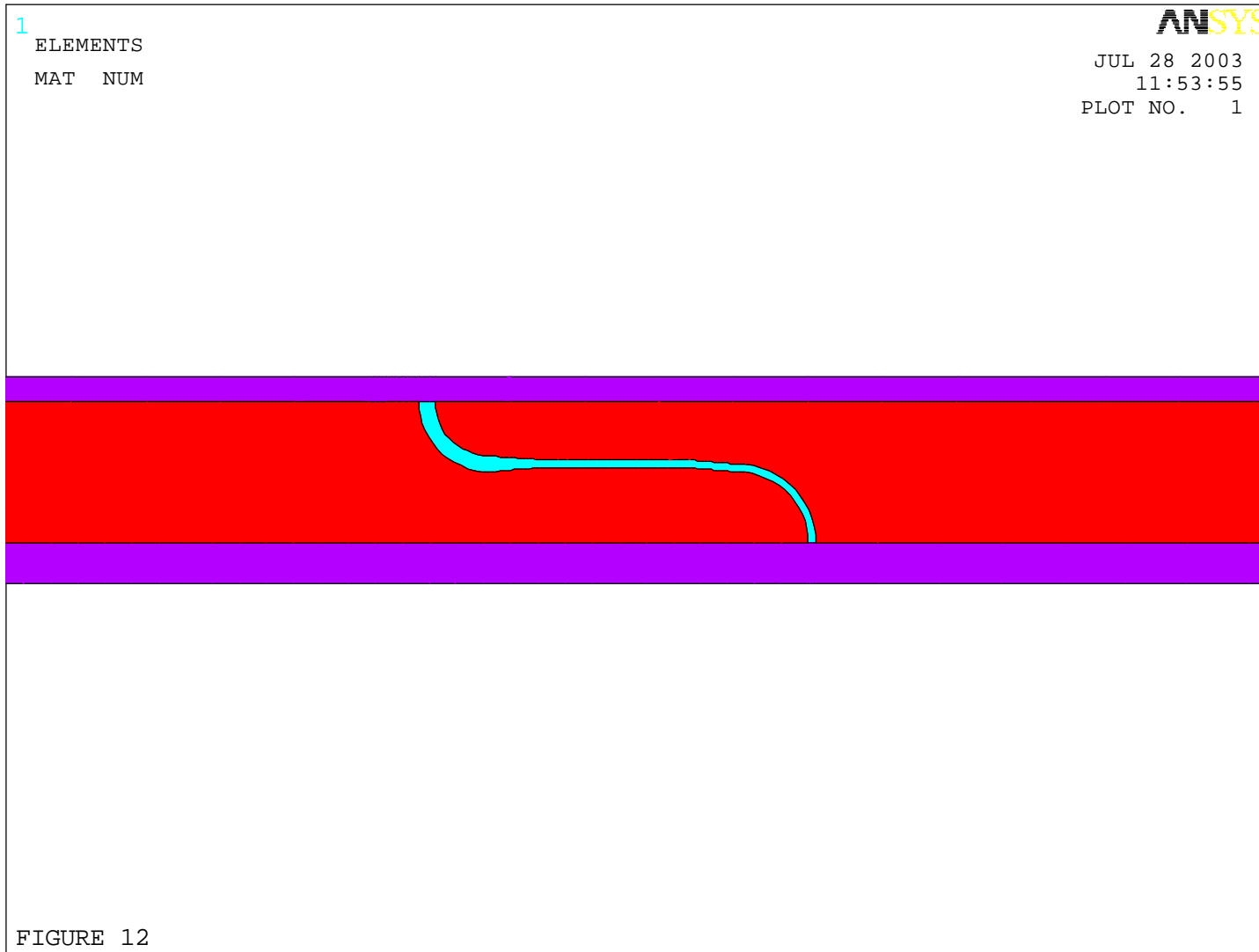
00048539

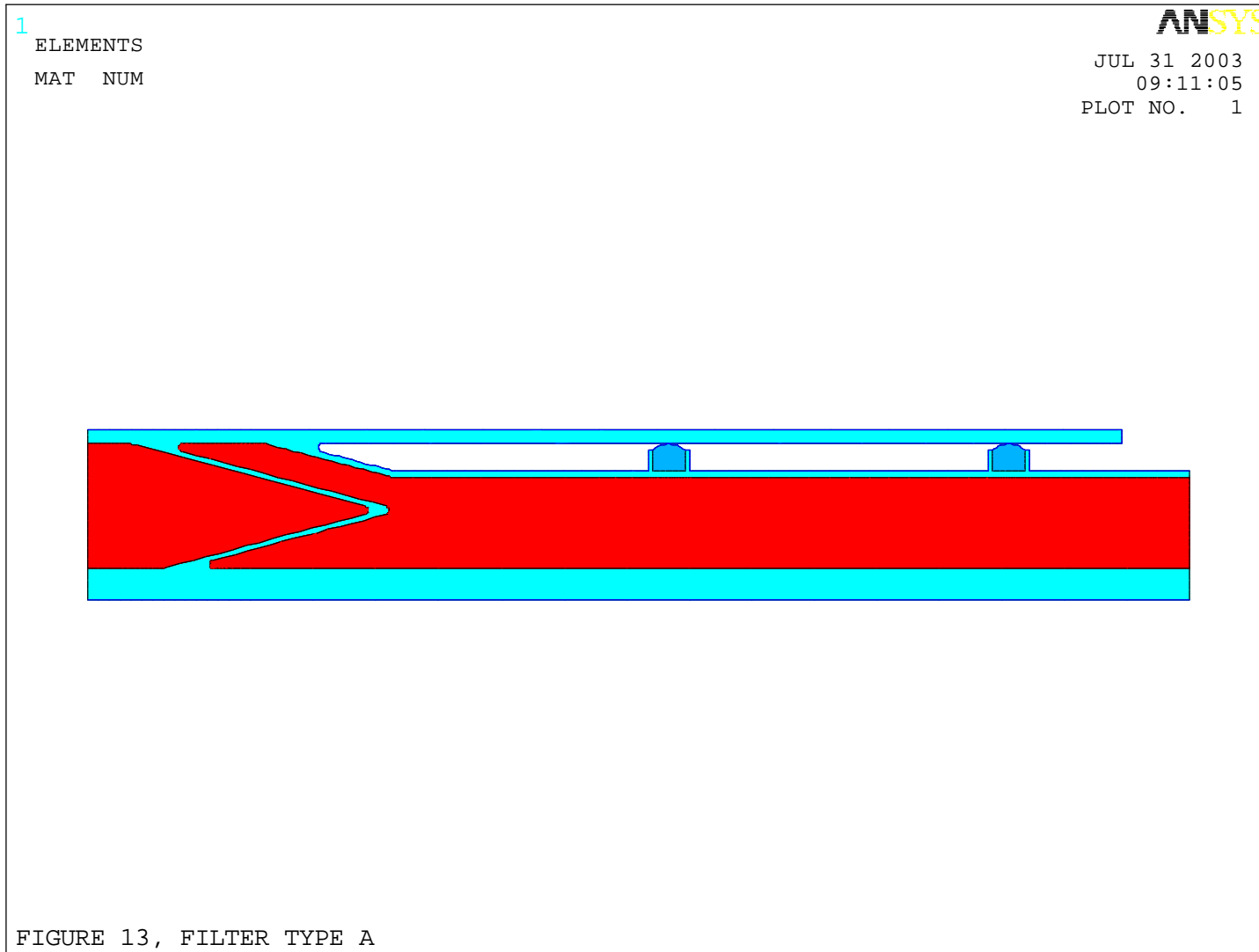






00048539





00048539

